iScience

CellPress
OPEN ACCESS

Article

Cryptocarya chinensis from the Upper Pleistocene of South China and its biogeographic and paleoecological implications

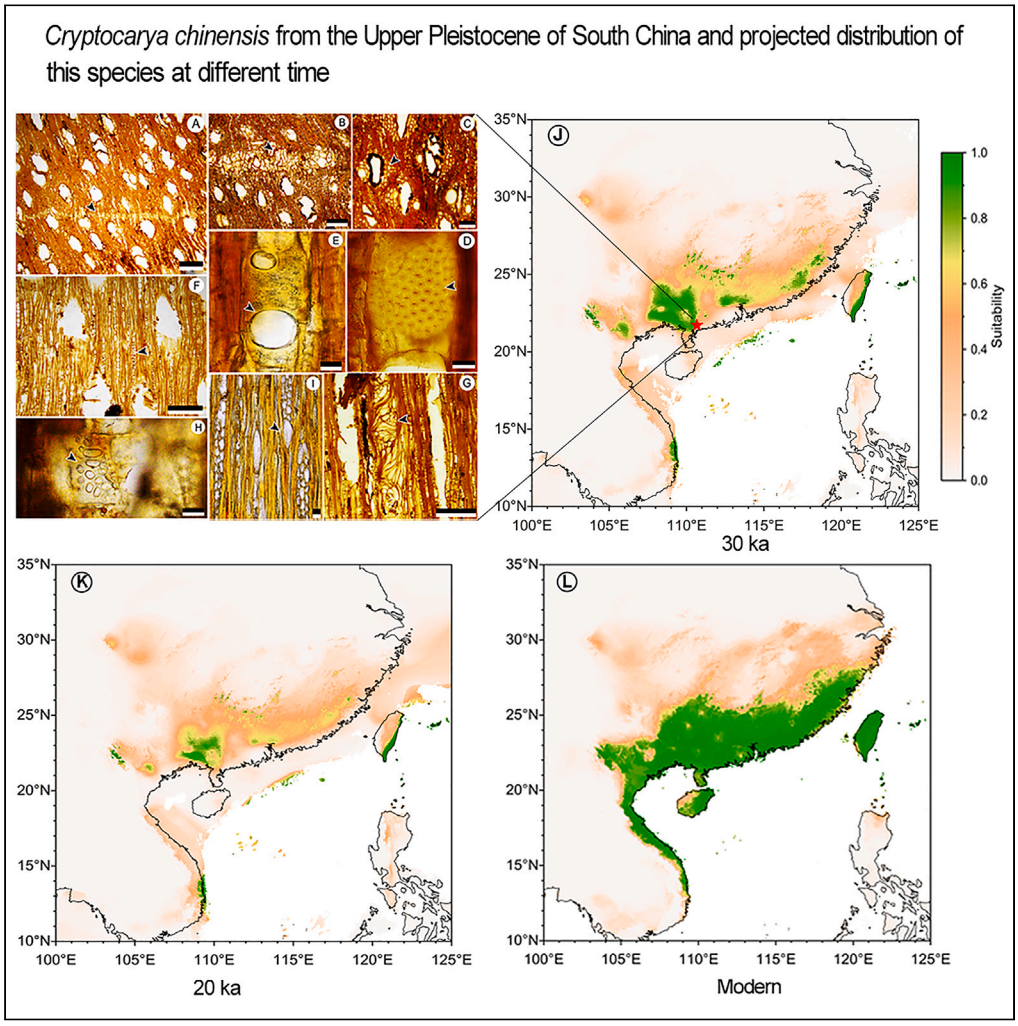

Lu-Liang Huang, Shu-Feng Li, Wei-Ye Huang, Jian-Hua Jin, Alexei A. Oskolski

571854202@qq.com (L.-L.H.)
lssjjh@mail.sysu.edu.cn (J.-H.J.)

Highlights

Fossil wood *C. chinensis* from the Upper Pleistocene of South China was presented

It represents the first reliable fossil record of *Cryptocarya* in Asia

Fossil combined with SDM show that modern *C. chinensis* in Maoming can be glacial relicts

Connection between *C. chinensis* and *Phytobia* flies persisted since the Late Pleistocene

Huang et al., iScience *26*, 107313
August 18, 2023
https://doi.org/10.1016/j.isci.2023.107313

iScience

CellPress
OPEN ACCESS

Article

Cryptocarya chinensis from the Upper Pleistocene of South China and its biogeographic and paleoecological implications

Lu-Liang Huang,[1,2,6,*] Shu-Feng Li,[3] Wei-Ye Huang,[1] Jian-Hua Jin,[1,*] and Alexei A. Oskolski[4,5]

SUMMARY

Anatomical structure of mummified wood of *Cryptocarya* (Lauraceae) from the Upper Pleistocene of Maoming, South China and the woods of 15 extant species of *Cryptocarya* from China and Malaysia were examined. The fossil wood has been convincingly attributed to extant species *Cryptocarya chinensis* (Hance) Hemsl. This is the first reliable fossil record of *Cryptocarya* in Asia. The finding combined with the results of Biomod2 species distribution modeling suggest that the range of *C. chinensis* in the Late Pleistocene in South China and North Vietnam was very restricted due to increased continental aridity and enhanced temperature seasonality in this region. Thus, modern populations of *C. chinensis* in Maoming can be considered as glacial relicts. The mines (larval tunnels) produced by the larvae of flies from the genus *Phytobia* Lioy (Agromyzidae, Diptera) were observed in fossil wood under study. These cambial miners have never been reported in *Cryptocarya*.

INTRODUCTION

The Lauraceae is one of the largest and most widespread plant families in moist subtropical and tropical regions of the Americas, Asia, and Australia,[1,2] comprising approximately 50 genera with 2500–3500 species, and with its highest species richness occurring in the tropical forests of Southeast Asia, and Central and South America.[3–5] This magnoliid angiosperm group is ancient, with fossil records dating back to the Late Cretaceous.[3] The origin of different Lauraceae genera was considered to be Laurasian (North American and Eurasian), e.g., for *Cinnamomum* Schaeff. and *Litsea* Lam.,[6] or Gondwanan, e.g., for *Cryptocarya* R. Br., *Endiandra* R. Br., and *Sassafras* J. Presl.[7–9] However, the biogeographic histories of many lineages in this family are hard to interpret, due to the difficulty in ascribing the megafossils to extant genera,[10] and also to poor preservation of Lauraceae pollen.[11]

Cryptocarya R. Br. is one of the most species-rich genera in Lauraceae,[9] encompassing about 200–250 species widespread in tropical and subtropical regions of all continents (except central Africa) with the center of modern diversity in Southeast Asia,[5,12] and 21 species in southern China.[4] *Cryptocarya* together with *Beilschmiedia* Nees and *Endiandra* R. Br. are placed into the *Cryptocarya* group, which was first recognized by Richter[13] on the basis of wood and bark anatomy. Recent molecular data[5,14] suggest that this group is one of the early divergent clades in Lauraceae. Although the Gondwanan origin of *Cryptocarya* is widely accepted,[9] the biogeographic history of this genus remains obscure due to the rarity of reliable fossil records of this genus, especially in Asia.

In Asia, the earliest fossils ascribed to *Cryptocarya* are the leaves from the middle Eocene of the Changchang Formation, Hainan, South China.[15] Such generic placement of these fossil leaves is, however, obscure, because of the lack of preserved cuticles recording butterfly-shaped stomatal ledges. The presence of such ledges is an important diagnostic feature for extant *Cryptocarya*.[16–18] Apart from that, *Cryptocarya*-like fossil fruits were described from the Middle Miocene of Fujian, southeastern China,[19] but their attribution to Lauraceae is not convincing enough due to their poor preservation. Finally, the fossil leaves ascribed to *Cryptocarya concinna* Hance have been reported from the Middle Pleistocene of Guangxi, South China.[20,21] This attribution to *Cryptocarya* is seemingly also doubtful, however, due to poor preservation and the absence of a description for the fossil leaves, and the butterfly-shaped stomatal ledges being not apparent in this fossil.

[1]State Key Laboratory of Biocontrol and Guangdong Provincial Key Laboratory of Plant Resources, School of Life Sciences/School of Ecology, Sun Yat-sen University, Guangzhou 510275, China

[2]State Key Laboratory of Palaeobiology and Stratigraphy, Nanjing Institute of Geology and Palaeontology, Chinese Academy of Sciences, Nanjing 210008, China

[3]CAS Key Laboratory of Tropical Forest Ecology, Xishuangbanna Tropical Botanical Garden, Chinese Academy of Sciences, Mengla 666303, China

[4]Department of Botany and Plant Biotechnology, University of Johannesburg, P. O. Box 524 Auckland Park, Johannesburg 2006, South Africa

[5]Komarov Botanical Institute of the Russian Academy of Sciences, Prof. Popov str. 2, 197376 St. Petersburg, Russia

[6]Lead contact

*Correspondence: 571854202@qq.com (L.-L.H.), lssjjh@mail.sysu.edu.cn (J.-H.J.)

https://doi.org/10.1016/j.isci.2023.107313

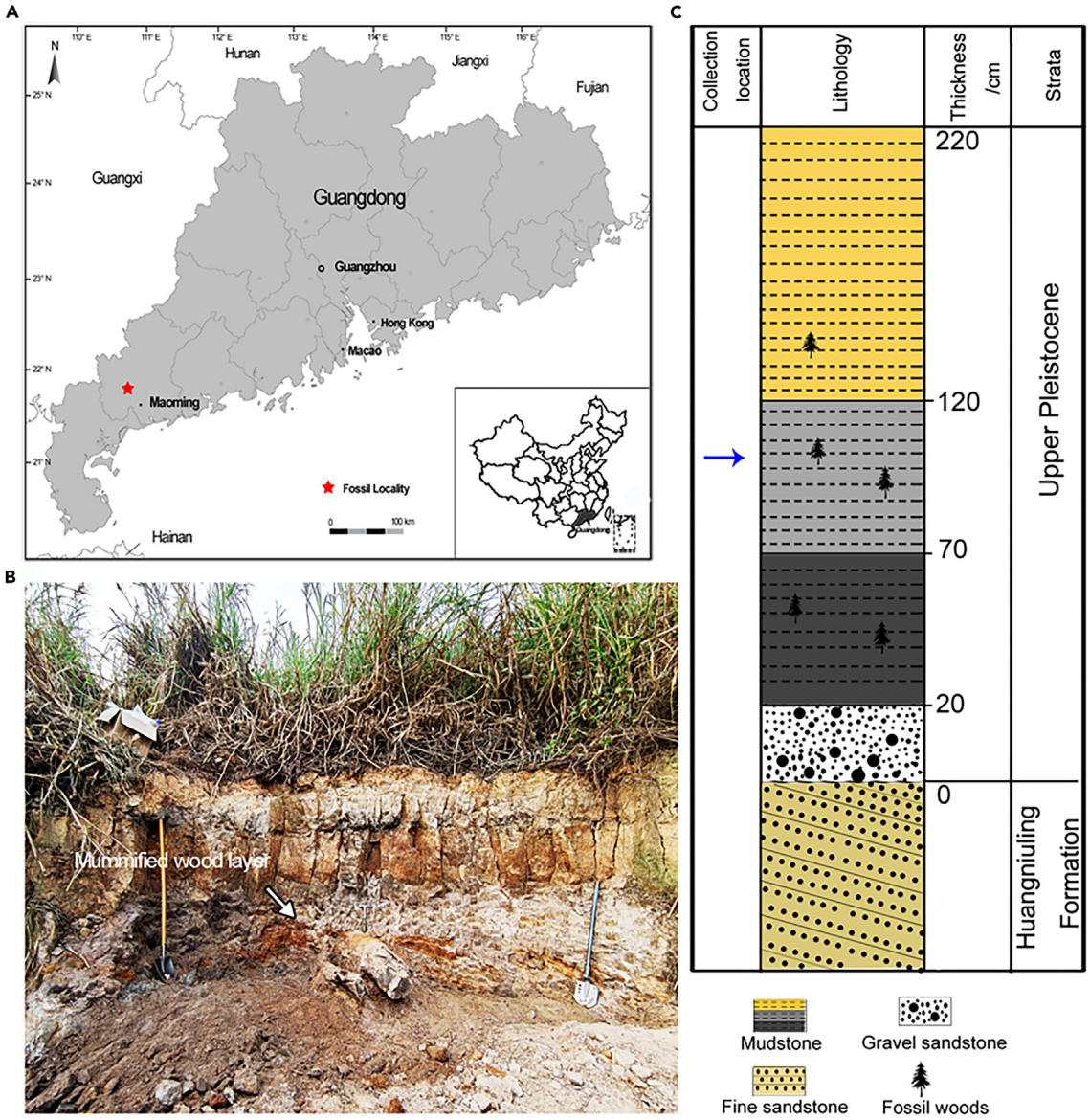

Figure 1. Geological setting of the mummified wood locality (modified from Huang et al.[25])

(A) Locality of the fossil woods (base map from d-maps: https://d-maps.com).

(B) Stratigraphic section of the Upper Pleistocene in the Maoming Basin.

(C) Lithological column of the fossiliferous deposit (Upper Pleistocene). The blue arrow indicates the layer in which the mummified woods were discovered.

In this paper, we described well-preserved mummified fossil woods of *Cryptocarya* from the Upper Pleistocene (i.e., 29–27 ka BP, 33–30 ka cal. BP) of the Maoming Basin, Guangdong, South China (Figure 1). It is worthy to note that the wood anatomy of extant eastern Asian species of *Cryptocarya* is still underexplored. Among 21 species of this genus occurring in China,[4] the data on wood structure are available only for *C. chingii* Cheng, *C. chinensis* (Hance) Hemsl., *C. densiflora* Bl., and *C. hainanensis* Merr.[22–24] Such scarce wood anatomical data are not sufficient for reliable identification of the fossil woods ascribed to this genus. To make the identification of the fossil wood from Maoming Basin more reliable, we examined the wood structure of 13 extant *Cryptocarya* species from China and 2 species from Malaysia.

Detailed comparison of the fossil wood from the Upper Pleistocene of Maoming Basin with available wood anatomical data for *Cryptocarya* strongly suggests its greatest affinity to the extant species *C. chinensis* (Hance) Hemsl.. We assert that this is the first megafossil found in Asia that can be assigned to *Cryptocarya*

with confidence. The finding of this species also enriches our view on the vegetation and environment of South China prior to the Last Glacial Maximum reconstructed on the basis of previous fossil data from the Maoming Basin.[25,26–30]

RESULTS

Systematic paleontology

Family: Lauraceae Juss.

Genus: *Cryptocarya* R. Br.

Species: *Cryptocarya chinensis* (Hance) Hemsl. (Figure 2)

Specimens: MMHW036, MMHW041, MMHW043.

Repository: The Museum of Biology, Sun Yat-sen University, Guangzhou, China.

Stratigraphic age: Late Pleistocene (29–27 ka BP, 33–30 ka cal. BP)

Locality: Maoming Basin, Guangdong, South China.

Description: Wood diffuse-porous. Growth ring boundaries indistinct or distinct, marked by 1−4-seriate marginal bands of axial parenchyma (Figure 2A). Vessels are angular to round in outline (Figures 2A–2C), solitary (40%), and 2–4 in a group; 41–174 μm (mean 91.8 ± 5.20 μm) in tangential diameter, 79–239 μm (mean 157.4 ± 7.15 μm) in radial diameter. Vessel frequency 14–22/mm^2 (mean 19/mm^2). Intervessel pits alternate and bordered (Figure 2D), polygonal to oval, 5.5–9.4 μm (mean 7.5 ± 0.17 μm) in horizontal size, and 5.5–9.4 μm (mean 7.7 ± 0.17 μm) in vertical size. Perforation plates simple (Figure 2E). Fibers libriform, with moderately thick walls, oval, square, or polygonal in cross section; pits on the walls are not observed. Fibers are mostly non-septate; septate fibers occasionally present. Axial parenchyma scanty paratracheal to vasicentric (rarely aliform) (Figure 2C) and in marginal or in seemingly marginal bands (Figures 2A), 1–4 cells wide. Rays heterocellular, 1–3-seriate (Figure 2F). Uniseriate rays mainly consist of square or upright cells. Biseriate and triseriate rays made of procumbent body cells with 1–4 rows of marginal square or upright cells. Rays 93–824 μm (mean 368.1 ± 25.95 μm) in height; 9–12 rays/mm. Aggregate rays are present (Figure 2G). Vessel-ray pits display much reduced borders to apparently simple: rounded or angular, horizontal (scalariform, gash-like) (Figure 2H), 2.7–13.5 μm (mean 7.3 ± 0.77 μm) in horizontal size, and 3.0–7.3 μm (mean 4.9 ± 0.23 μm) in vertical size. Oil/mucilage cells present, associated with ray parenchyma cells (Figure 2I). No crystals found in the cells of rays or axial parenchyma. The rounded to tangentially elongated pith flecks (Figure 2B) made of callus cells of irregular shape occur in the latewood of the studied wood samples.

Extant woods structure of *Cryptocarya* (Lauraceae) from China and Malaysia

Examined samples: *Cryptocarya brachythyrsa* H. W. Li (XTBG-00,2003,0995); *C. calcicola* H. W. Li (XTBG-00,2009,0262); *C. chinensis* (Hance) Hemsl. (CAFw16669); *C. chingii* Cheng (CAFw12894); *C. concinna* Hance (CAFw6492); *C. densiflora* Bl. (CAFw12151); *C. depauperata* H. W. Li (XTBG-00,2010,0462); *C. griffithii* Wight (CAFw6548); *C. hainanensis* Merr. (CAFw12182); *C. impressinervia* H. W. Li (CAFw12873); *C. kwangtungensis* H. T. Chang (XTBG-00,1960,0042); *C. maculata* H. W. Li (XTBG-00,2002,3291); *C. metcalfiana* Allen (CAFw17698); *C. wrayi* Gamble (XTBG-11,2001,0082); *C. yunnanensis* H. W. Li (XTBG-38,1997,0078). The quantitative anatomical data of these woods are shown in Tables 1 and S1.

Description: Wood diffuse-porous. Growth rings absent (*C. wrayi*) (Figure 3A) or distinct, marked by 2–4 rows of radially flattened fibers in *C. hainanensis* and *C. impressinervia* (Figure 3B), or marked by 1−4-seriate marginal bands of axial parenchyma in *C. chinensis*, *C. brachythyrsa*, *C. calcicola*, *C. chingii*, *C. concinna*, *C. densiflora*, *C. depauperata*, *C. kwangtungensis*, *C. maculata*, *C. metcalfiana*, *C. yunnanensis*, and *C. griffithii* (Figure 3C). Vessel lumina medium, 25–90 μm (average 47.7–65.8 μm) in tangential diameter in *C. brachythyrsa*, *C. calcicola*, *C. depauperata*, *C. maculata*, *C. wrayi*, and *C. yunnanensis*, and medium to large in other species, up to 35–146 μm (average 95.7–97.0 μm) in *C. densiflora*, *C. griffithii*, and *C. metcalfiana*, rounded in outline, solitary, and 2–4 in a group (Figures 3A–3F). Vessel frequency mostly 20−40 vessels/mm^2, with much more numerous vessels in *C. calcicola* (42−55 vessels/mm^2) and less numerous in *C.*

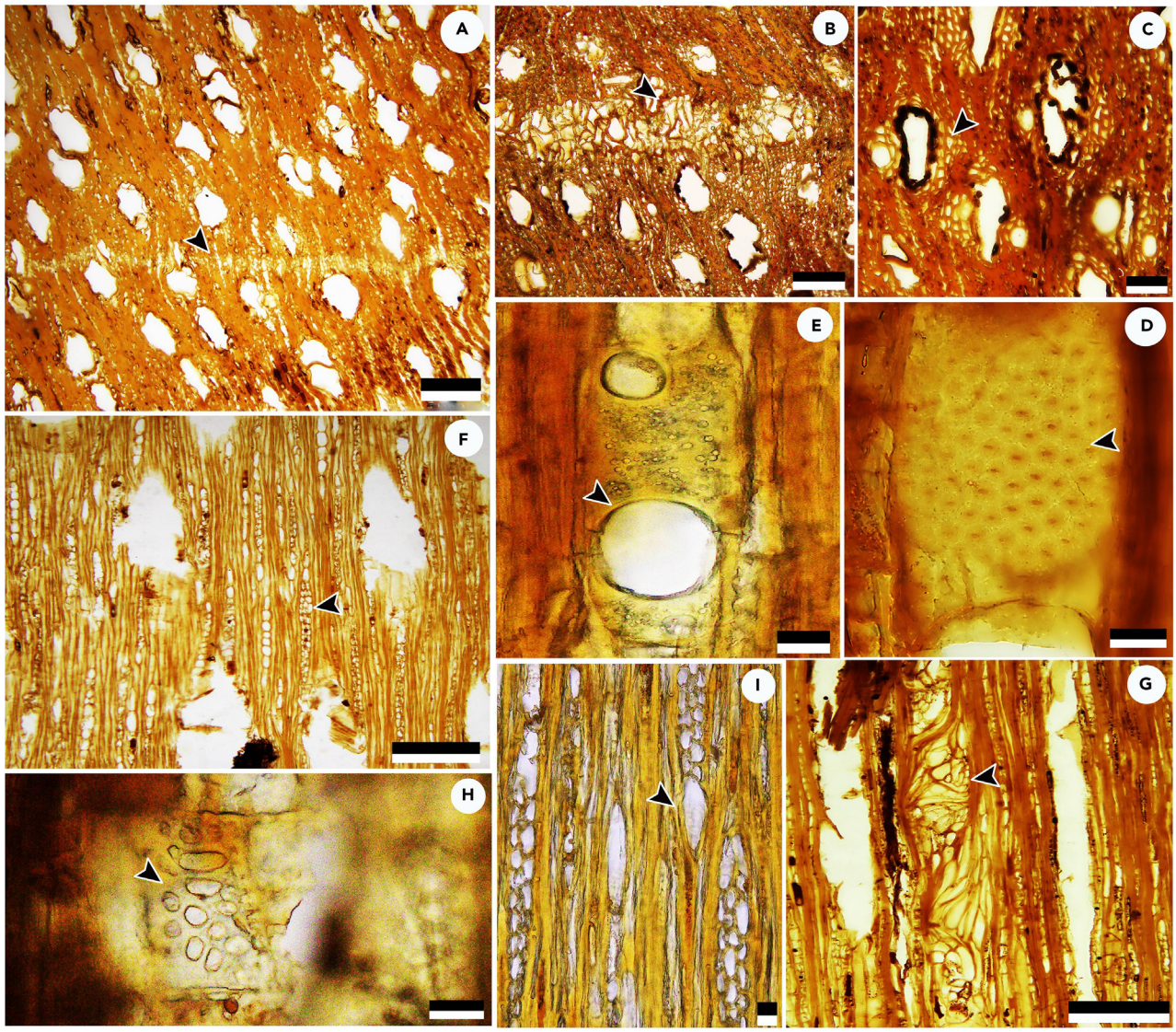

Figure 2. Wood structure of *Cryptocarya chinensis* (Hance) Hemsl. from Maoming (MMHW041)

(A) Transverse section showing diffuse-porous wood, growth rings absent or indistinct; axial parenchyma in seemingly marginal bands (marked by arrowheads).

(B) Showing pith flecks in cross section (marked by arrowheads).

(C) Axial parenchyma scanty paratracheal to vasicentric, occasional aliform (marked by arrowheads).

(D) Bordered intervessel pits alternate (marked by arrowheads).

(E) Simple perforation plates (marked by arrowheads).

(F) Rays 1–3-seriate in width (marked by arrowheads).

(G) Tangential section showing aggregate rays (marked by arrowheads).

(H) Vessel-ray pits with much reduced borders to apparently simple: round to oval or horizontally elongated to scalariform (marked by arrowheads).

(I) Oil/mucilage cells associated with ray cells (marked by arrowheads). Scale bars: A, B, F, G 200 μm; C 100 μm; D, E, H, I 20 μm.

wrayi and *C. griffithii* (≤10 vessels/mm^2). Intervessel pits alternate and bordered (Figure 4A), polygonal to oval, medium to large (range 5.2–16.1 μm in horizontal size and 4.9–15.0 μm in vertical size). Perforation plates mostly simple (Figure 4B); but scalariform perforation plates with up to 9 bars rarely occur in *C. impressinervia* and *C. hainanensis* (Figure 4C). Fibers moderately thick-walled, oval, square, or polygonal in cross section, with simple to minutely bordered pits on radial walls (distinctly bordered pits occasionally occur in *C. chinensis* and *C. concina*). Fibers are mostly non-septate; septate fibers occur in all species, but the most common in *C. hainanensis* and *C. wrayi* (Figure 4D). Axial parenchyma scanty paratracheal to

Table 1. Quantitative anatomical data for wood of *Cryptocarya* (Lauraceae) from China and Malaysia

Species and collection numbers	1	2	3	4	5	6	7	8	9
Cryptocarya brachythyrsa (XTBG-00,2003,0995)	50.3 ± 12.99 26–78	27 21–30	8.0 ± 0.86 5.9–9.7	7.4 ± 0.72 5.9–9.0	5	10–13	9.3 ± 3.16 4.9–16.4	7.2 ± 1.39 4.9–9.1	298.0 ± 117.70 55–841
C. calcicola (XTBG-00,2009,0262)	51.4 ± 15.64 27–81	48 42–55	7.3 ± 0.72 5.6–8.5	6.9 ± 1.00 5.0–8.7	3	7–10	11.58 ± 4.69 5.7–19.2	5.8 ± 1.26 4.3–9.1	435.7 ± 256.76 78–1174
C. chinensis (CAFw16669)	89.6 ± 20.60 41–116	20 17–24	9.8 ± 1.30 7.7–12.0	10.0 ± 1.30 7.7–12.5	3	6–11	19.4 ± 8.98 6.3–39.7	8.7 ± 1.78 4.6–12.5	280.0 ± 16.9.0 44–774
C. chingii (CAFw12894)	93.0 ± 20.73 38–125	17 14–24	13.2 ± 1.23 10.9–16.0	12.8 ± 1.36 9.8–15.0	5	8–11	12.3 ± 4.74 3.5–24.0	8.9 ± 2.10 5.5–13.4	441.1 ± 192.90 80–939
C. concinna (CAFw6492)	83.9 ± 12.77 51–105	18 10–23	9.6 ± 1.04 7.5–11.5	9.9 ± 1.18 7.2–12.9	3	6–8	14.1 ± 6.28 3.8–27.0	9.2 ± 2.51 5.3–16.2	311.4 ± 157.90 34–8639
C. densiflora (CAFw12151)	95.9 ± 22.94 31–143	21 17–26	12.4 ± 0.90 11.2–14.5	11.4 ± 1.24 9.8–14.3	3	6–10	16.0 ± 6.88 7.4–29.6	9.8 ± 2.14 7.1–14.5	268.4 ± 157.92 34–863
C. depauperata (XTBG-00,2010,0462)	49.8 ± 14.04 32–80	24 21–26	8.8 ± 0.95 7.1–11.2	7.5 ± 0.89 5.7–9.0	3	8–11	14.5 ± 6.28 3.8–27.0	7.4 ± 1.32 5.0–10.0	381.8 ± 249.15 130–1022
C. griffithii (CAFw6548)	97.0 ± 30.70 47–143	8 5–10	13.2 ± 1.19 11.0–16.1	12.4 ± 1.26 9.1–15.0	4	6–8	21.0 ± 7.53 7.0–32.1	9.8 ± 3.27 5.1–19.3	388.0 ± 155.60 89–732
C. hainanensis (CAFw12182)	95.6 ± 13.70 64–125	24 20–28	6.9 ± 0.85 5.4–8.7	6.4 ± 0.66 4.9–7.3	3	5–8	11.8 ± 6.43 5.2–36.8	6.6 ± 1.02 4.3–8.7	242.5 ± 107.19 34–479
C. impressinervia (CAFw12873)	71.8 ± 13.77 44–97	36 30–40	6.8 ± 0.83 5.2–8.7	6.7 ± 0.64 5.7–8.1	3	6–9	10.3 ± 7.07 5.5–35.1	5.5 ± 0.72 4.1–7.3	360.4 ± 169.61 45–764
C. kwangtungensis (XTBG-00,1960,0042)	73.5 ± 20.78 37–121	18 17–20	10.4 ± 1.05 8.4–12.6	10.0 ± 0.93 8.0–11.9	5	7–10	8.5 ± 2.68 5.1–16.1	7.6 ± 1.64 4.0–11.2	293.0 ± 148.96 34–657
C. maculata (XTBG-00,2002,3291)	47.7 ± 14.30 27–83	41 34–49	8.9 ± 1.13 6.4–11.8	8.4 ± 1.19 6.1–11.0	3	10–14	15.8 ± 7.10 7.8–32.2	7.3 ± 1.65 2.8–9.6	378.3 ± 163.11 64–777
C. metcalfiana (CAFw17698)	96.1 ± 24.59 35–146	17 17–20	10.7 ± 0.811 9.0–12.2	11.4 ± 0.90 9.4–12.8	4	5–8	10.7 ± 4.84 5.4–23.2	11.1 ± 3.79 7.2–21.9	390.0 ± 172.47 108–758
C. wrayi (XTBG-11,2001,0082)	60.1 ± 12.96 40–88	8 7–10	9.8 ± 1.04 7.7–12.3	7.4 ± 1.11 5.6–10.1	3	10–13	12.1 ± 4.78 5.3–25.7	8.6 ± 3.71 5.0–17.8	295.6 ± 207.10 47–857
C. yunnanensis (XTBG-38,1997,0078)	65.8 ± 14.25 35–91	26 22–28	9.7 ± 1.12 7.4–12.4	8.7 ± 0.87 7.1–11.2	4	7–12	11.5 ± 4.79 5.1–22.3	6.2 ± 1.46 3.5–8.5	399.4 ± 134.67 117–804

1, Tangential diameter of vessels (average/min–max, μm). 2, Number of vessels per mm^2 (average/min–max). 3, Horizontal size of intervessel pits (average/min–max, μm). 4, Vertical size of intervessel pits (average/min–max, μm). 5, Width of rays (max, cells). 6, Number of rays per mm. 7, Horizontal size of vessel-ray pits (average/min–max, μm). 8, Vertical size of vessel-ray pits (average/min–max, μm). 9, Height of rays (average/min–max, μm).

vasicentric in *C. hainanensis*, *C. impressinervia*, and *C. wrayi* (Figures 3B and 3D), vasicentric to aliform and confluent, marginal or in seemingly marginal bands in *C. concinna* (Figure 3E) and *C. yunnanensis*, scanty paratracheal to vasicentric and marginal or in seemingly marginal bands (1–4 cells wide) in other samples (Figure 3F). Rays heterocellular, up to 3-seriate in *C. chinensis*, *C. calcicola*, *C. concinna*, *C. densiflora*, *C. depauperata*, *C. hainanensis*, *C. impressinervia*, *C. maculata*, and *C. wrayi* (Figure 4E); up to 4-seriate in *C. metcalfiana*, *C. yunnanensis*, and *C. griffithii*; up to 5-seriate in *C. brachythyrsa*, *C. chingii*, and *C. kwangtungensis* (Figure 4F); aggregate rays occur in *C. chinensis*, *C. densiflora*, and *C. kwangtungensis* (Figures 4E–4G). Uniseriate rays are mainly consist of square or/and upright cells. Multiseriate rays made of procumbent body cells with 1–4 rows of marginal square or upright cells. Rays usually less than 0.9 mm in height, taller rays more than 1 mm occur in *C. calcicola* and *C. depauperata* (Figure 4H). Vessel-ray pits display much reduced borders to apparently simple: rounded or angular, horizontal (scalariform, gash-like) to vertical (palisade) (Figure 5A), 3.5–39.7 μm in horizontal size and 2.8–21.9 μm in vertical size. Oil/mucilage cells associated with ray parenchyma occur in *C. chinensis*, *C. chingii*, *C. densiflora*, *C. hainanensis*, *C. impressinervia*, *C. kwangtungensis*, *C. metcalfiana*, *C. yunnanensis*, *C. wrayi*, and *C. griffithii* (Figure 5B); those associated with axial parenchyma are found in *C. hainanensis*, *C. impressinervia*, *C. kwangtungensis*, *C. metcalfiana*, and *C. griffithii* (Figure 5C), and those scattered among fibers were observed in *C. densiflora*, *C. griffithii*, *C. hainanensis*, *C. impressinervia*, *C. kwangtungensis*, and *C.*

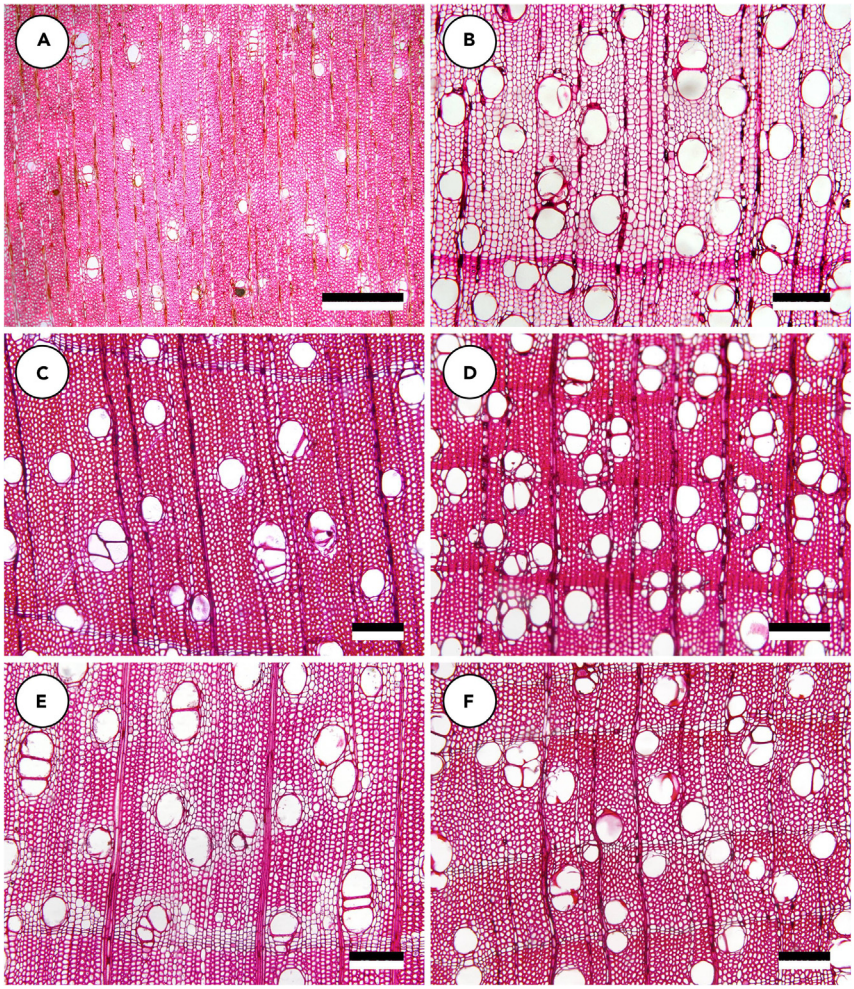

Figure 3. Wood structure of extant *Cryptocarya* species, transverse sections

(A) *C. wrayi*, growth rings absent.

(B) *C. hainanensis*, growth ring boundary marked by 2–4 rows of radially flattened fibers, scanty paratracheal axial parenchyma.

(C) *C. chinensis*, growth ring boundary marked by 1–4-seriate band of axial parenchyma; scanty paratracheal axial parenchyma.

(D) *C. impressinervia*, growth ring boundary marked by 2–4 rows of radially flattened fibers, scanty paratracheal to vasicentric axial parenchyma.

(E) *C. concina*, axial parenchyma vasicentric, aliform to confluent, marginal bands.

(F) *C. densiflora*, axial parenchyma scanty paratracheal to vasicentric and in 2–4-seriate marginal bands. Scale bars: A 500 μm; B–F 200 μm.

yunnanensis (Figure 5D). Prismatic crystals present in ray cells of *C. brachythyrsa*, *C. chingii*, *C. depauperata*, *C. maculata*, *C. metcalfiana* (Figure 5E), and absent in other samples. Helical thickenings not found.

Comparison with modern woods

The InsideWood[23] search with the combination of exclusively simple perforation plates (13p14a); alternate intervessel pitting (22p); round to oval vessel-ray pits with much reduced borders to apparently simple (31p); vasicentric and marginal axial parenchyma (79p89p); up to 3-seriate rays (97p98a); oil/mucilage cells associated with ray cells (124p); and the absence of crystals (136a) returns only the members of Lauraceae, such as *Aniba canelilla* (HBK) Mez., *A. ferrea* Kubitzki, *Beilschmiedia* sp., *Cryptocarya chinensis*, *C. enervis* Hook. f., *Licaria subbullata* Kosterm, and several species of *Dehaasia* Blume. Among these species, only *C. chinensis* has oil/mucilage cells confined to ray parenchyma whereas other taxa also show the association

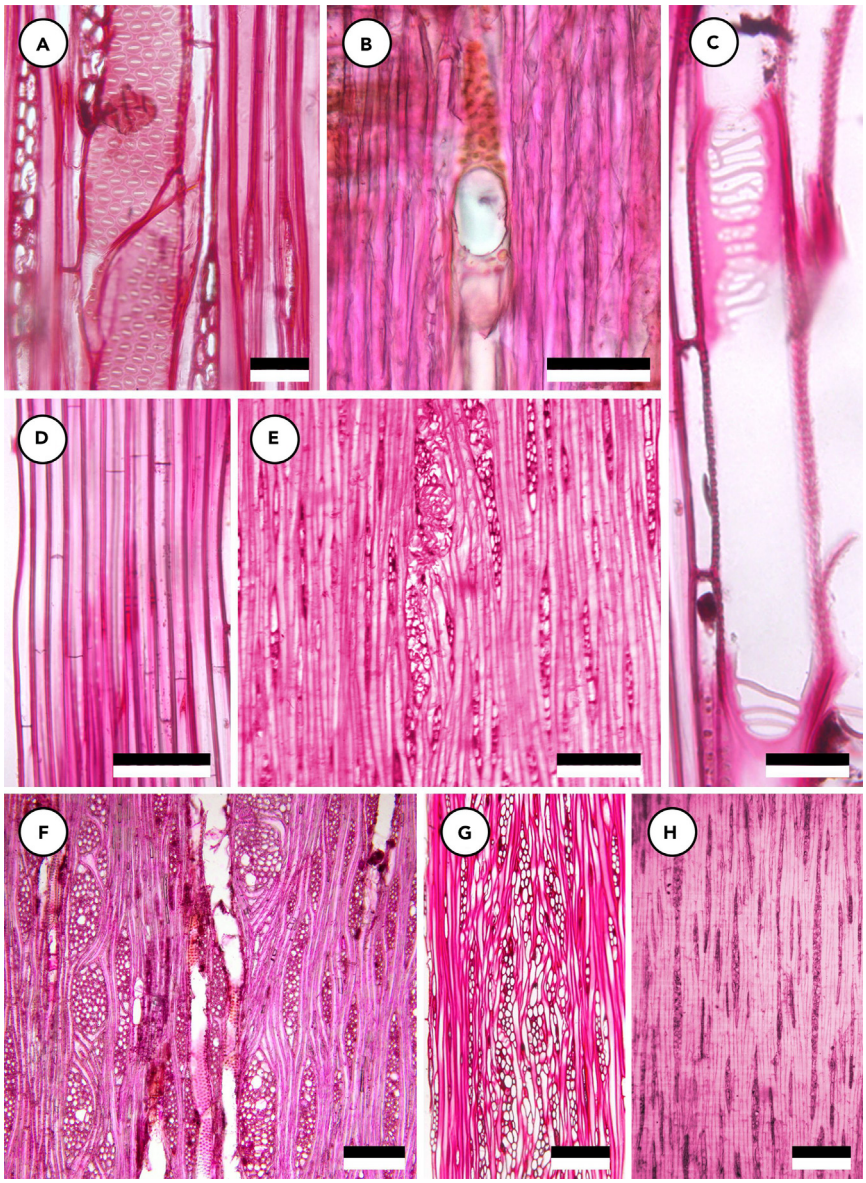

Figure 4. Wood structure of extant *Cryptocarya* species, longitudinal sections

Wood structure of extant *Cryptocarya* species, longitudinal tangential (A, E–H), and radial (B–D) sections.
(A) *C. chinensis*, alternate intervessel pitting.
(B) *C. chinensis*, simple perforation plate.
(C) *C. hainanensis*, scalariform perforation plates.
(D) *C. hainanensis*, septate libriform fibers abundant.
(E) *C. chinensis*, 1–3-seriate and aggregate rays.
(F) *C. kwangtungensis*, 1–5-seriate and aggregate rays.
(G) *C. densiflora*, aggregate rays.
(H) *C. depauperata*, 1–3-seriate rays, tall ray >1 mm in height. Scale bars: A–C 50 μm; D 100 μm; E–H 200 μm.

of these cells with axial parenchyma. Apart from that, the occurrence of oil/mucilage cells among the fibers has been reported in *Beilschmiedia* sp. and *Dehaasia*.[13,23,31–34] In addition, *Beilschmiedia* sp. differs from the fossil wood in having confluent axial parenchyma.[32] The results of the InsideWood search as well as our observations suggest, therefore, that the fossil wood under study shows the greatest resemblance to the genus *Cryptocarya*.

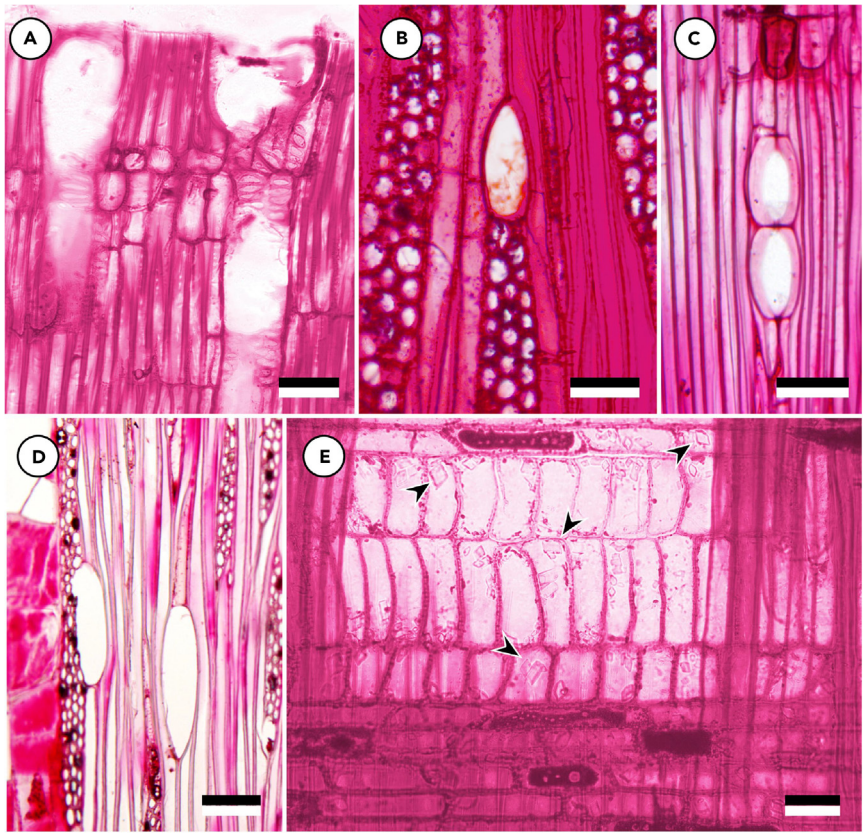

Figure 5. Details of wood structure in extant *Cryptocarya* species, longitudinal sections

Details of wood structure in extant *Cryptocarya* species, longitudinal radial (A, C, E) and tangential (B, D) sections.
(A) *C. chinensis*, horizontal (scalariform) vessel-ray pits with much reduced borders to apparently simple.
(B) *C. chinensis*, oil/mucilage cells associated with ray parenchyma.
(C) *C. hainanensis*, oil/mucilage cells associated with a strand of axial parenchyma.
(D) *C. griffithii*, oil/mucilage cells among fibs.
(E) *C. chingii*, ray with procumbent body cells and upright cells in marginal rows, prismatic crystal in upright ray cells marked by arrowheads. Scale bars: A, C, D 100 μm; B, E 50 μm.

Among extant species of this genus, the combination of narrow (1–3-seriate) rays with the occurrence of oil/mucilage cells in ray parenchyma has been reported in *C. alba* (Mol.) Looser,[35] *C. crassifolia* Baker,[23] *C. diversifolia* Blume (Table 2),[33] *C. enervis* Hook. f.,[33] *C. konishii* Hay, and *C. chinensis* (Table 2),[36,37] as well as in *C. hainanensis*, *C. impressinervia*, and *C. wrayi* based on our examination of some extant woods structure of this genus from China and Malaysia (Table 2). Unlike the fossil woods under study, however, *C. alba* has prismatic crystals in ray cells and the common occurrence of radial multiples vessels. The Pleistocene woods from Maoming are distinctive from *C. konishii*, *C. impressinervia*, and *C. hainanensis* in terms of the lack of scalariform perforation plates;[36] it also differs from *C. crassifolia*, *C. diversifolia*, *C. hainanensis*, *C. impressinervia*, and *C. enervis* by the absence of oil/mucilage cells associated with axial parenchyma, or occurring among fibers. Apart from that, *C. diversifolia* has larger intervessel pits (11.2–14.5 μm in horizontal size) than the fossil wood from Maoming; *C. hainanensis*, *C. impressinervia*, and *C. wrayi* differ from the latter one by lacking marginal bands of axial parenchyma, whereas *C. wrayi* has lower vessel frequency (7–10 vessels/mm^2) than the studied fossil wood (Table 2). Finally, the wood from Maoming is distinctive from all previously mentioned *Cryptocarya* species except *C. chinensis* in having the aggregate rays. It is worthy to mention that although Itoh et al.[24] reported that the occurrence of oil cells is associated with axial parenchyma in *C. chinensis*, the results of our observation showed that oil cells occur exclusively in the ray parenchyma of this species.

Thus, the fossil woods under study show the greatest similarity to *C. chinensis*, which is confirmed by comparing sections of extant wood of this species obtained from the Wood Collection of the Chinese

Table 2. Some extant woods structure of *Cryptocarya* (Lauraceae) from China and Malaysia

Species and collection numbers	Scalariform perforation plates	Axial parenchyma				Ray width (cells)	Location of oil cells			Crystals in rays	Aggregate rays	Septate fibers	Notes
		Scanty paratracheal	Vasicentric	Aliform/ confluent	Marginal bands		with ray cells	with axial parenchyma	with fiber				
Cryptocarya brachythyrsa (XTBG-00,2003,0995)	–	+	+	–	+	1–5	–	–	–	+	–	rare	
C. calcicola (XTBG-00,2009,0262)	–	+	+	–	+	1–3	–	–	–	–	–	rare	
C. chinensis (CAFw16669)	–	+	+	–	+	1–3	+	–	–	–	+	rare	Oil cells is only associated with axial parenchyma[24]
C. chingii (CAFw12894)	–	+	+	–	+	1–5	+	–	–	+	–	rare	Oil cells is only associated with axial parenchyma[22]
C. concinna (CAFw6492)	–	–	+	+	+	1–3	–	–	–	–	–	rare	
C. densiflora (CAFw12151)	–	+	+	–	+	1–3	+	–	+	–	+	rare	Oil cells is only associated with axial parenchyma[24]
C. depauperata (XTBG-00,2010,0462)	–	+	+	–	+	1–3	–	–	–	+	–	rare	
C. griffithii (CAFw6548)	–	+	+	–	+	1–4	+	+	+	–	–	rare	
C. hainanensis (CAFw12182)	+	+	+	–	–	1–3	+	+	+	–	–	common	Oil cells is only associated with axial parenchyma[24]
C. impressinervia (CAFw12873)	+	+	+			1–3	+	+	+	–	–	rare	
C. kwangtungensis (XTBG-00,1960,0042)	–	+	+	–	+	1–5	+	+	+	–	+	rare	
C. maculata (XTBG-00,2002,3291)	–	+	+	–	+	1–3	–	–	–	+	–	rare	
C. metcalfiana (CAFw17698)	–	+	+	–	+	1–4	+	+	–	+	–	rare	
C. wrayi (XTBG-11,2001,0082)	–	+	+	–	–	1–3	+	–	–	–	–	common	
C. yunnanensis (XTBG-38,1997,0078)	–	–	+	+	+	1–4	+	–	+	–	–	rare	

Notes: (+) present, (–) absent, (?) no data.

Academy of Forestry (catalog No. CAFw16669). On the basis of these comparisons, we can attribute the Late Pleistocene wood from the Maoming Basin to *C. chinensis* with confidence.

Comparison with other fossil woods

The fossil woods under study are diffuse-porous (5p); have exclusively simple perforation plates (13p14a); alternate intervessel pitting (22p); round to oval vessel-ray pits with much reduced borders to apparently simple (300p); a lack of helical thickenings (36a); axial parenchyma in seemingly marginal bands (89p); 1–3-seriate rays (97p); oil/mucilage cells associated with ray cells (124p); and an absence of crystals (136a). An InsideWood[23] search for a combination of these traits returns fossil woods of *Erythrophloemoxylon scholleri* Boureau placed to Fabaceae[38] and six taxa assigned to Lauraceae, i.e., *Laurinoxylon nectandrioides* Kräusel & Schonfeld,[39] *Rosarioxylon bajacaliforniensis* Cevallos-Ferriz, Catharina & Kneller,[40] *Ulminium magnioleiferum* Wheeler & Manchester,[41] *Cryptocaryoxylon grandoleaceum* Akkemik,[42] *C. lesbium* Mantzouka,[43] and *C. radiporosum* Wheeler & Manchester.[41] Unlike the fossil wood from Maoming, however, *Erythrophloemoxylon scholleri*, *Laurinoxylon nectandrioides*, and *Ulminium magnioleiferum* share the oil/mucilage cells both associated with axial parenchyma and among fibers. Apart from that, *E. scholleri* may be distinguished by its normal axial canals and storied rays, whereas *Laurinoxylon nectandrioides* and *Ulminium magnioleiferum* differ from the fossil sample under study in having wider (>3-seriate) rays. *Rosarioxylon bajacaliforniensis* possesses predominantly radial multiples of 2–7 vessels, and larger intervessel pits (>10 μm) than the fossil woods of Maoming.

Thus, the fossil woods from Maoming show the most similarity to fossil woods ascribed to the genus *Cryptocaryoxylon* Leisman,[44] sharing distinctive features such as marginal or apparently marginal bands of axial parenchyma, exclusively simple perforation plates, and oil/mucilage cells associated with rays.[43] *Cryptocaryoxylon grandoleaceum*, *C. lesbium*, and *C. radiporosum* share, however, a higher vessel frequency (>30 vessels/mm^2) than the studied fossil wood. *C. lesbium* and *C. radiporosum* are also have larger intervessel pits (>10 μm in diameter) than the Pleistocene wood from Maoming, whereas *C. grandoleaceum* and *C. radiporosum* are also distinct from the Pleistocene wood from Maoming in terms of the occurrence of oil/mucilage cells among fibers. The fossil woods from Maoming also show great similarity to *Cryptocaryoxylon irregularis* Akkemik, Iamandei & Çelik,[45] whereas the latter has higher vessel frequency (42–65 vessels/mm^2) than the studied fossil woods; besides, all rays of *C. irregularis* are procumbent and its vessels are mostly radial multiples (>90%).

In summary, the Late Pleistocene fossil woods from Maoming are the most similar to the extant species *C. chinensis* (Hance) Hemsl. and the fossil woods of *Cryptocaryoxylon* Leisman. Thus, we ascribed the fossil woods under study to *C. chinensis* (Hance) Hemsl.

Climatic data for the Late Pleistocene (30 ka and 20 ka) and modern Maoming

The values of bioclimatic variables for modern climate prevailing at the fossil locality (21.87°N, 110.67°E), their ranges for the modern distribution of *C. chinensis* extracted from the WorldClim database (see Table S2) as well as their values for the Late Pleistocene (30 ka and 20 ka) reconstructed by the Oscillayers datasets at the closest locality to the fossil site (22.50°N, 112.50°E), and the climatic ranges estimated by Coexistence Approach (CA) for the Late Pleistocene (33–30 ka) in the Maoming Basin[30] are collated in the Table 3. The CA estimations are based on the overlapping modern distribution areas of *Pinus armandii*, *P. hwangshanensis*, *Liquidambar formosana*, and *Keteleeria davidiana* whose fossils were also found at the same site.[25,26,29,30]

As these data show, all parameters of the Late Pleistocene climate reconstructed for the Maoming Basin are within the ranges of respective bioclimatic variables for the modern distribution area of *C. chinensis*. The Late Pleistocene climate in this locality was, however, somewhat drier than that found in most modern localities of this species, as the ranges of the precipitation variables (BIO12–BIO14 and BIO16–BIO19) suggest. The modern climate in the Maoming Basin shows high values of BIO5 (maximum temperature of warmest month), BIO8 (mean temperature of wettest quarter), and BIO10 (mean temperature of warmest quarter), which are nearly limiting for *C. chinensis*. Such hot summer seasons potentially threaten the continued survival of this species in South China.

Model performance and suitable habitats of *C. chinensis* in the present and past

Among the five algorithms (see Figure S1), the random forest model had the best performance (TSS = 0.9833, ROC = 0.9112), followed by general boosted model, maximum entropy (MaxEnt. Phillips. 2), flexible

Table 3. The comparison of bioclimatic variables for the Late Pleistocene (30 ka and 20 ka) and modern Maoming Basin with the ranges of modern *Cryptocarya chinensis*

Climate Variables	33–30 ka Coexistence Approach	30 ka Oscillayers	20 ka Oscillayers	Modern	The range of modern *C. chinensis*
Annual mean temperature, °C (BIO1)	10.8–22.2	19.24	19.97	23.20	12.6–25.7
Mean diurnal range, °C (BIO2)	6.8–7.9	8.73	8.44	7.10	5.2–9.2
Isothermality (BIO3)	23–33	36.67	38.22	34.00	22–52
Temperature seasonality (BIO4)	5723–8732	5356.89	4937.78	4827.00	2533–8612
Max. temperature of warmest month, °C (BIO5)	24.3–33.6	29.93	29.76	32.40	19.7–33.9
Minimum temperature of coldest month, °C (BIO6)	−3.9–9.5	6.43	7.93	11.80	1.2–17.4
Temperature annual range, °C (BIO7)	23.3–32.5	23.47	21.82	20.60	14.0–31.7
Mean temperature of wettest quarter, °C (BIO8)	18.1–28.1	23.99	25.67	28.60	15.4–28.6
Mean temperature of driest quarter, °C (BIO9)	2.6–15.8	15.31	13.96	18.00	4.7–27.2
Mean temperature of warmest quarter, °C (BIO10)	20.2–28.5	25.42	25.67	28.60	16.0–28.8
Mean temperature of coldest quarter, °C (BIO11)	1.4–14.1	11.71	12.98	16.40	4.7–21.8
Annual precipitation, mm (BIO12)	1313–2014	1513.56	1404.56	1629.00	1117–4448
Precipitation of wettest month, mm (BIO13)	200–329	262.56	259.78	306.00	177–1019
Precipitation of driest month, mm (BIO14)	32–51	20.22	15.33	25.00	7–214
Precipitation seasonality (BIO15)	49–65	73.33	79.33	71.00	15–107
Precipitation of wettest quarter, mm (BIO16)	555–841	729.44	714.44	795.00	512–2682
Precipitation of driest quarter, mm (BIO17)	114–191	81.22	62.33	98.00	32–773
Precipitation of warmest quarter, mm (BIO18)	508–841	692.67	714.44	795.00	435–2682
Precipitation of coldest quarter, mm (BIO19)	114–219	122.44	75.44	101.00	33–995

The Late Pleistocene climate data were reconstructed by Coexistence Approach (CA) based on Maoming fossil data,[30] modeling by Oscillayers datasets (ages 30 ka BP and 20 ka BP, 22.50°N, 112.50°E), the modern climate data at the fossil locality (21.87°N, 110.67°E) and climate variables within the range of modern *C. chinensis* were both extracted from the WorldClim data.

discriminant analysis, and multiple adaptive regression splines. The results obtained for the percent contribution of climatic variables reveal that the most important climatic variables affecting shifts in species distributions of *C. chinensis* in the ensemble model were mean diurnal range (BIO2), temperature seasonality (BIO4), isothermality (BIO3) as well as the precipitation of coldest quarter (BIO19) and of warmest quarter (BIO18), annual precipitation (BIO12), precipitation of wettest month (BIO13), precipitation seasonality (BIO15), and the mean temperature of wettest quarter (BIO8) with importance scores of 0.54, 0.33, 0.17, 0.16, 0.13, 0.12, 0.10, 0.05, and 0.04, respectively (see Figure S2).

The response curves of 9 variables regarding *C. chinensis* from MaxEnt. Phillips. 2, which represent the quantitative relationship between environmental variables and habitat suitability, are shown in Figure S3. Based on the response curves, the likely suitable ranges of BIO2 ranged from 5 to 9.3 if the threshold of 0.6 was chosen, while 50 to 75 were the most suitable values of BIO2 for *C. chinensis*. For BIO4, the suitable range was 6000–13000 with a threshold of 0.6. When BIO3 is larger than 35, habitat suitability increases dramatically (threshold is 0.6). The habitat suitability shows negative relationships with BIO8, BIO12, and BIO13. A positive relationship between habitat suitability and BIO18 was observed.

The Biomod2 ensemble model run for *C. chinensis* (Figure 6A) showed that under today's climate, in addition to the modern distribution areas of this species, highly climatically suitable habitats (suitability>0.8) were also observed in other areas in southern China (notably Guizhou, Jiangxi, Yunnan, and Jiangsu provinces), as well as in Vietnam.

The projections of climatically suitable habitats for *C. chinensis* at 20 ka (Last Glacial Maximum) and 30 ka (Figures 6B and 6C) indicate that highly suitable habitats (suitability >0.8) were observed only in some areas of Guangxi, Guangdong, Taiwan, Fujian, Hunan, and Sichuan in southern China, as well as a few areas in Vietnam. It is clear that climatically suitable habitats for this species during the last glaciation show great

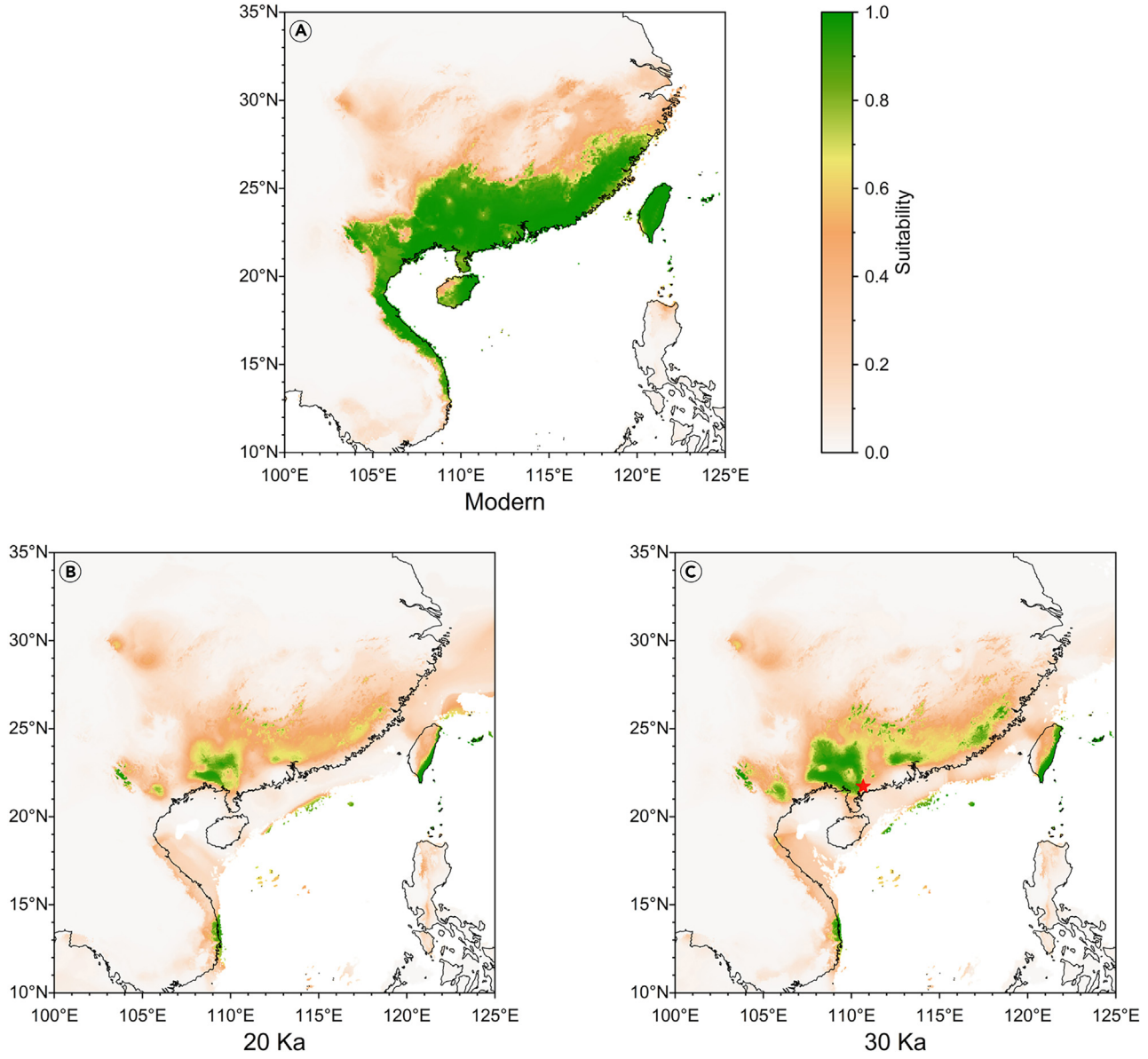

Figure 6. Projected suitable habitats for *Cryptocarya chinensis* at different time

(A) Modern projected climatically suitable habitats for *C. chinensis*.

(B) Projected climatically suitable habitats for *C. chinensis* at 20 ka.

(C) Projected climatically suitable habitats for *C. chinensis* at 30 ka. The red star indicates the fossil locality.

range contraction compared to the present (Figures 6B and 6C). However, the Maoming fossil locality remained within the highly climatically suitable habitat range for *C. chinensis* during this period.

DISCUSSION

Paleoecological implications

C. chinensis from Maoming (Guangdong Province) is the earliest fossil of *Cryptocarya* in Eastern Asia (Figure 7, see Table S3). The assignment of previous fossils to *Cryptocarya* in this region is doubtful (see the review in the introduction) and mostly ancient fossils showing more certain affinity to this genus have been found in the Southern Hemisphere (Figure 7, see Table S3). These new fossils from Maoming show that *Cryptocarya* must have inhabited Asia in the Late Pleistocene, even in the relatively cool conditions of the last glaciation.

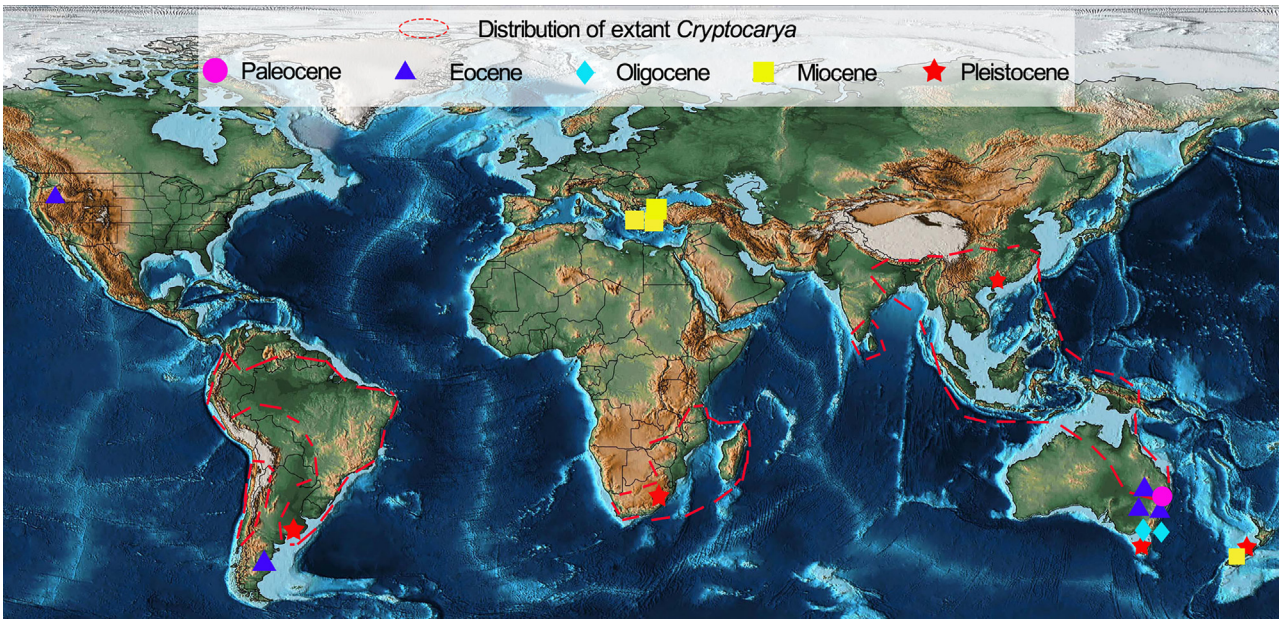

Figure 7. The distribution of extant and reliable fossil records of *Cryptocarya* or its relevant taxa

The finding of fossil wood of *C. chinensis* in the Late Pleistocene deposits of the Maoming Basin is entirely consistent with the results of the Biomod2 ensemble SDM showing that this region was among only a few areas suitable for this species prior the Last Glacial Maximum (30 ka). The SDM also showed that BIO2, BIO4, BIO3, and BIO19 as well as BIO18 are the most important bioclimatic variables influencing the distribution of *C. chinensis*. This suite of climatic parameters suggests that the range of this species in the Late Pleistocene was restricted due to increased continental aridity and enhanced temperature seasonality in subtropical South China. Apparently, these climatic changes manifested an intensification of the winter monsoon and a weakening of the summer monsoon compared to now, which is typical for the transition from interglacial to glacial regimes in this region.[46] At the same time, the values of all bioclimatic variables estimated for the Maoming Basin using different paleoclimatic proxies for the period from the Late Pleistocene to the present do not exceed the ranges of respective parameters within the modern distribution area of *C. chinensis* (Table 3, see Table S2). It is highly likely that the Maoming Basin is a relic locality for this species that has persisted there at least since the Late Pleistocene. A phylogeographic analysis of genetic diversity within the populations of *C. chinensis* from different parts of its distribution range is required to test this hypothesis.

The pith flecks found in the studied woods (Figure 2B), as well as in modern wood of *C. chinensis*,[36] evidence the activity of cambium-mining insects.[47–49] The tangentially stretched pith flecks observed in the woods from the Late Pleistocene of the Maoming Basin are typical for the mines (larval tunnels) produced by the larvae of flies from the genus *Phytobia* Lioy (Agromyzidae, Diptera).[47,49–51] Unlike the parenchymatic clusters of frost traumatic origin, these structures in the fossil sample show certain resemblance to larval tunnels by their elliptic to elongated shape on transverse section, irregular arrangement of callus cells, and by their localization in the latewood.[51] *Phytobia* larvae have been found in the wood of not fewer than 13 modern genera of Lauraceae.[52] However, these cambial miners have never been reported in *Cryptocarya*, and the *Phytobia* species feeding on the extant *C. chinensis* have not been identified. Nevertheless, our data show that the association between *C. chinensis* and *Phytobia* flies has persisted since the Late Pleistocene.

Limitations of the study

Although the phytogeographical history of *Cryptocarya* plants based on fossil records has been reviewed in this study, paleobotanical research is almost always limited by the fossils being studied. Firstly, the number and botanical details preserved in the plant fossils are limited. Second, the representativeness of these fossil records, which affect how phytogeographical history can be interpreted. In addition, the limitations of Biomod2 ensemble SDM modeling in the current study include data accuracy, the representativeness of

the fossils in relation to the once-living source material, and spatiotemporal bias, which are believed to be common limitations associated with SDMs. More reliable fossils and additional methods are important to explore a more accurate historical biogeography of plants in the past.

STAR★METHODS

Detailed methods are provided in the online version of this paper and include the following:

- KEY RESOURCES TABLE
- RESOURCE AVAILABILITY
  - Lead contact
  - Materials availability
  - Data and code availability
- EXPERIMENTAL MODEL AND SUBJECT DETAILS
  - Plants
- METHODS DETAILS
  - Geological setting
  - Taxonomic validation of fossil woods and terminology
  - Wood anatomical study of extant *cryptocarya* species from China and Malaysia
- QUANTIFICATION AND STATISTICAL ANALYSIS
  - Climatic data collection
  - Biomod2 ensemble species distribution modeling
  - Climatic variable processing
  - Model establishment

SUPPLEMENTAL INFORMATION

Supplemental information can be found online at https://doi.org/10.1016/j.isci.2023.107313.

ACKNOWLEDGMENTS

This study was supported by the National Natural Science Foundation of China (Grant nos. 42102004, 42072020); the China Postdoctoral Science Foundation (Grant no. 2020M683027), the State Key Laboratory of Palaeobiology and Stratigraphy (Nanjing Institute of Geology and Palaeontology, Chinese Academy of Sciences) (Grant no. 223110), the Young and Middle-aged Academic and Technical Leaders of Yunnan (Grant no. 202305AC160051) and the Fundamental Research Funds for the Central Universities (Grant no. 22qntd2606). We thank the University of Johannesburg and the Komarov Botanical Institute (institutional research project no. AAAA-A19-119030190018-1) for financial support for A.A.O. We are grateful to Mr. Yonggang Zhang from Wood Collection of Research Institute of Wood Industry, Chinese Academy of Forestry; the Paleoecology Research Group and Center for Gardening and Horticulture, Xishuangbanna Tropical Botanical Garden, Chinese Academy of Sciences for providing the wood samples and sections of extant *Cryptocarya* for anatomical comparison. We are grateful to Prof. Robert A. Spicer (The Open University, UK) for improvements to the English in this paper.

AUTHOR CONTRIBUTIONS

J.-H.J. directed in the design of the study. L.-L.H., J.-H.J., and A.A.O. carried out anatomical examination of fossil and extant woods of *Cryptocarya*. L.-L.H., S.-F.L., W.-Y.H., J.-H.J., and A.A.O. conducted the taxonomic assessment of the fossil sample, its paleoclimate and Biomod2 SDMs interpretations. L.-L.H., W.-Y.H., and A.A.O. photographed the specimens and constructed the figures. L.-L.H. and A.A.O. wrote the manuscript and formatted the text.

DECLARATION OF INTERESTS

The authors declare no conflict of interest.

Received: February 7, 2023
Revised: May 25, 2023
Accepted: July 4, 2023
Published: July 10, 2023

REFERENCES

1. Gentry, A.H. (1988). Changes in plant community diversity and floristic composition on environmental and geographical gradients. Ann. Mo. Bot. Gard. *75*, 1–34.

2. van der Werff, H., and Richter, H.G. (1996). Toward an improved classification of Lauraceae. Ann. Mo. Bot. Gard. *83*, 409–418.

3. Rohwer, J.G. (1993). Lauraceae. In The Families and Genera of Vascular Plants II Flowering Plant, Dicotyledons, Magnoliid, Hamamelid and Caryophyllid Families. 366–391, K. Kubitzki, J.G. Rohwer, and V. Bittrich, eds. (SpringerVerlag).

4. Li, X.W., Li, J., Huang, P.H., Wei, F.N., Cui, H.B., and van der Werff, H. (2008). Lauraceae. In Flora of China 7: 102–254, Z.Y. Wu and P. Raven, eds. (Beijing: Science Press and St. Louis: Missouri Botanical Garden).

5. Rohwer, J.G., De Moraes, P.L.R., Rudolph, B., and van der Werff, H. (2014). A phylogenetic analysis of the *Cryptocarya* group (Lauraceae), and relationships of Dahlgrenodendron, Sinopora, Triadodaphne and Yasunia. Phytotaxa *158*, 111–132.

6. Huang, J.F., Li, L., van der Werff, H., Li, H.-W., Rohwer, J.G., Crayn, D.M., Meng, H.H., van der Merwe, M., Conran, J.G., and Li, J. (2016). Origins and evolution of cinnamon and camphor: A phylogenetic and historical biogeographical analysis of the *Cinnamomum* group (Lauraceae). Mol. Phylogenet. Evol. *96*, 33–44.

7. Poole, I., Richter, H.G., and Francis, J.E. (2000). Evidence for Gondwana origins for *Sassafras* (Lauraceae)? Late Cretaceous fossil wood of Antarctica. IAWA J. *21*, 463–475.

8. Chanderbali, A.S., van der Werff, H., and Renner, S.S. (2001). Phylogeny and historical biogeography of Lauraceae: evidence from the chloroplast and nuclear genomes. Ann. Mo. Bot. Gard. *88*, 104–134.

9. Van der Merwe, M., Crayn, D.M., Ford, A.J., Weston, P.H., and Rossetto, M. (2016). Evolution of Australian *Cryptocarya* (Lauraceae) based on nuclear and plastid phylogenetic trees: evidence of recent landscape-level disjunctions. Aust. Syst. Bot. *29*, 157–166.

10. Carpenter, R.J., Truswell, E.M., and Harris, W.K. (2010). Lauraceae fossils from a volcanic Palaeocene oceanic island, Ninetyeast Ridge, Indian Ocean: ancient long-distance dispersal? J. Biogeogr. *37*, 1202–1213.

11. Kooyman, R.M., Morley, R.J., Crayn, D.M., Joyce, E.M., Rossetto, M., Slik, J.F., Strijk, J.S., Su, T., Yap, J.Y.S., and Wilf, P. (2019). Origins and Assembly of Malesian Rainforests. Annu. Rev. Ecol. Evol. Syst. *50*, 119–143.

12. De Kok, R.P.J. (2015). A revision of *Cryptocarya* (Lauraceae) from Thailand and Indochina. Gardens' Bulletin Singapore *67*, 309–350.

13. Richter, H.G. (1981). Anatomie des sekundären Xylems und der Rinde der Lauraceae (Paul Parey).

14. Rohwer, J.G. (2000). Toward a phylogenetic classification of the Lauraceae: Evidence from matK sequences. Syst. Bot. *25*, 60–71.

15. Li, J.Z. (2010). Eocene Lauraceae Plants from Changchang Basin, Hainan Island of China and Its Paleoenvironment Significance. PhD Thesis (Sun Yat-sen University). (In Chinese).

16. Christophel, D.C., and Rowett, A.I. (1996). Leaf and Cuticle Atlas of Australian Leafy Lauraceae (Australian Biological Resources Study).

17. Christophel, D.C., Kerrigan, R., and Rowett, A.I. (1996). The use of cuticular features in the taxonomy of the Lauraceae. Ann. Mo. Bot. Gard. *83*, 419–432.

18. Nishida, S., Kok, R.D., and Yang, Y. (2016). Cuticular features of *Cryptocarya* (Lauraceae) from Peninsular Malaysia, Thailand and Indo-China and its taxonomic implications. Phytotaxa *244*, 26–44.

19. Wang, Y., Jia, J., Wang, Y., Li, F., Song, X., Qin, S., Wang, Z., Kitazato, K., and Wang, Y. (2019). New fossil leaves and fruits of Lauraceae from the Middle Miocene of Fujian, southeastern China differentiated using a cluster analysis. Crit. Rev. Microbiol. *45*, 581–594.

20. Liu, Y.S. (1993). A palaeoclimatic analysis on early Pleistocene flora of Changsheling Formation, Baise Basin, Guangxi. Acta Palaeontol. Sin. *32*, 151–169. (In Chinese, with English abstract).

21. Liu, Y.C., and Quan, C. (2017). Late Cenozoic climates of low-latitude East Asia: A paleobotanical example from the Baise Basin of Guangxi, southern China. Palaeoworld *26*, 572–580.

22. Cheng, J.Q., Yang, J.J., and Liu, P. (1992). Chinese Woods (Chinese Forestry Publishing House). (in Chinese).

23. InsideWood (2004-onwards). Published on the internet. http://insidewood.lib.ncsu.edu/search.

24. Itoh, T., Pan, B., Youzou, S., Pieter, B., Luo, J.Y., Li, D.G., Cui, Y.Z., Wang, F., Mechtild, M., Tomoyuki, F., et al. (2022). Anatomical Database and Atlas of Chinese Woods (Kaiseisha Press).

25. Huang, L.L., Jin, J.H., and Oskolski, A.A. (2021a). Mummified fossil of *Keteleeria* from the Late Pleistocene of Maoming Basin, South China, and its phytogeographical and paleoecological implications. J. Systemat. Evol. *59*, 198–215.

26. Huang, L.L., Jin, J.H., Quan, C., and Oskolski, A.A. (2021b). New occurrences of Altingiaceae fossil woods from the Miocene and Upper Pleistocene of South China with phytogeographic implications. J. Palaeogeogr. *10*, 482–493.

27. Xiang, H., Kodrul, T.M., Romanov, M.S., Maslova, N.P., Han, M., Huang, L., Wu, X., and Jin, J. (2022). Mummified fruits of *Canarium* from the upper Pleistocene of South China. iScience *25*, 105385.

28. Xiang, H., Wu, X., Liu, X., Xu, S., Jin, J., and Huang, L. (2023). The first fossil seed of *Ampelopsis* (Vitaceae) in South China. Front. Ecol. Evol. *11*, 1130586.

29. Bazhenova, N.V., Wu, X.K., Kodrul, T.M., Maslova, N.P., Tekleva, M.V., Xu, S.L., and Jin, J.H. (2022). Mummified Seed Cones of *Pinus prehwangshanensis* sp. nov. (Subgenus *Pinus*, Pinaceae) From the Upper Pleistocene of Guangdong, South China: Taxonomical Significance and Implication for Phytogeography and Ecology. Front. Ecol. Evol. *10*, 900687.

30. Huang, L., Li, S., Huang, W., Xiang, H., Jin, J., and Oskolski, A.A. (2023). Glacial expansion of cold-tolerant species in low latitudes: megafossil evidence and species distribution modelling. Natl. Sci. Rev. *10*, nwad038.

31. Richter, H.G. (1985). Wood and bark anatomy of Lauraceae. II. Licaria Aublet. IAWA Bull. n.s. *6*, 187–199.

32. Detienne, P., and Jacquet, P. (1983). Atlas didentification des bois de l'Amazonie et des régions voiseines (Centre Technique Forestier Tropical).

33. Ogata, K., and Kalat, A. (1997). Wood Anatomy of Some Trees, Shrubs and Climbers in Brunei Darussalam. After-Care Programme, Brunei Forestry Research Project Special Publication No. 3 (Japan International Cooperation Agency (JICA) and Forestry Department, Ministry of Industry and Primary Resources, Brunei Darussalam).

34. Sosef, M.S.M., Hong, L.T., and Prawirohatmodjo, S. (1998). Plant Resources of South-East Asia. No. 5 (3). Timber Trees: Lesser-Known Timbers (Backhuys Publishers).

35. Rancusi, M.H., Nishida, M., and Nishida, H. (1987). Xylotomy of the important Chilean woods. In Contributions to the Botany in the Andes II. 68–153, M. Nishida, ed. (Academia Scientific Book Inc).

36. Kanehira, R. (1921). Anatomical Characters and Identification of Formosan Woods with Critical Remarks from the Climatic Point of View (Bureau of Productive Industries, Government of Formosa).

37. Itoh, T. (1996). In Anatomical description of Japanese hardwoods II. Wood Research and Technical Notes, *32*, pp. 66–89, (In Japanese).

38. Müller-Stoll, W.R., and Mädel, E. (1967). Die fossilen Leguminosen-Hölzer. Eine Revision der mit Leguminosen verglichenen fossilen Hölzer und Beschreibung älterer und neuer Arten. Palaeontographica *119B*, 95–174.

39. Van der Burgh, J. (1964). Hölzer der Niederrheinishen Braunkohlenformation. 1. Hölzer der Braunkohlengrube "Anna" zu Haanrade (Niederlandisch Limburg). Acta Bot. Neerl. *13*, 250–301.

40. Cevallos-Ferriz, S.R., Catharina, A.S., and Kneller, B. (2021). Cretaceous Lauraceae

wood from El Rosario, Baja California, Mexico. Rev. Palaeobot. Palynol. *292*, 104478.

41. Wheeler, E.A., and Manchester, S.R. (2002). Woods of the Eocene Nut Beds flora, Clarno Formation, Oregon, USA. IAWA Journal, 188.

42. Akkemik, Ü. (2021). A re-examination of the angiosperm wood record from the early and middle Miocene of Turkey. Acta Palaeobot. *61*, 42–94.

43. Mantzouka, D. (2018). The first report of *Cryptocaryoxylon* from the Neogene (Early Miocene) of Eurasia (eastern Mediterranean: Lesbos and Lemnos Islands, Greece). Fossil Imprint *74*, 29–36.

44. Leisman, G.A. (1986). *Cryptocaryoxylon gippslandicum* gen. et sp. nov., from the Tertiary of eastern Victoria. Alcheringa *10*, 225–234.

45. Akkemik, Ü., Iamandei, S., and Çelik, H. (2022). Further contribution to the early Miocene woody flora of Galatian Volcanic Provincefrom Doğanyurt Village, Ankara (Turkey). Turk. J. Earth Sci. *31*, 208–234.

46. Wang, L., Sarnthein, M., Erlenkeuser, H., Grimalt, J., Grootes, P., Heilig, S., Ivanova, E., Kienast, M., Pelejero, C., and Pflaumann, U. (1999). East Asian monsoon climate during the Late Pleistocene: High-resolution sediment records from the South China Sea. Mar. Geol. *156*, 245–284.

47. Süss, H. (1979). Durch *Protophytobia cupressorum* gen. nov., sp. nov. (Agromyzidae, Diptera) verursachte Markflecke in einem Holz von Juniperoxylon aus dem Tertiär von Süd-Limburg (Niederlande) und der Nachweis von Markflecken in einer rezenten Callitris-Art. Feddes Repert. *90*, 165–172.

48. Ishihama, N., Fu, K.K., and Ohtani, J. (1993). Observations on the occurrence of pith flecks of some hardwoods in Hokkaido and notes on some cambium miners. Res. Bull. Hokkaido Univ. For. *501*, 161–177. (In Japanese).

49. Winkler, I.S., Labandeira, C.C., Wappler, T., and Wilf, P. (2010). Distinguishing Agromyzidae (Diptera) leaf mines in the fossil record: new taxa from the Paleogene of North America and Germany and their evolutionary implications. J. Paleontol. *84*, 935–954.

50. Gregory, R., and Wallner, W. (1979). Histological relationship of *Phytobia setosa* to *Acer saccharum*. Can. J. Bot. *57*, 403–407.

51. Bonham, V.A., and Barnett, J.R. (2001). Formation and structure of larval tunnels of *Phytobia betulae* in *Betula pendula*. IAWA J. *22*, 289–294.

52. Spencer, K.A. (1990). Host Specialization in the World Agromyzidae (Diptera) (Dordrecht: Kluwer Academic Publishers).

53. Nan, Y., and Zhou, G.Q. (1996). Stratigraphy (Lithostratic) of Guangdong Province. Multiple Classification and Correlation of the Stratigraphy of China, *44* (China University Geosciences Press).

54. Herman, A.B., Spicer, R.A., Aleksandrova, G.N., Yang, J., Kodrul, T.M., Maslova, N.P., Spicer, T.E., Chen, G., and Jin, J.H. (2017). Eocene–early Oligocene climate and vegetation change in southern China: Evidence from the Maoming Basin. Palaeogeogr. Palaeoclimatol. Palaeoecol. *479*, 126–137.

55. Jin, J.H., Herman, A.B., Spicer, R.A., and Kodrul, T.M. (2017). Palaeoclimate background of the diverse Eocene floras of South China. Sci. Bull. *62*, 1501–1503.

56. Taylor, T.N., Krings, M., and Taylor, E.L. (2015). Fossil Fungi (Academic Press).

57. Lin, J.X. (1993). Notes on the improvements of wood sectioning techniques. Chin. Bull. Bot. *10*, 61–64. (In Chinese).

58. IAWA Committee (1989). IAWA list of microscopic features for hardwood identification. IAWA Bull. n. s. *10*, 219e332.

59. Wheeler, E.A. (2011). InsideWood: A web resource for hardwood anatomy. IAWA J. *32*, 199–211.

60. Wheeler, E.A., Gasson, P.E., and Baas, P. (2020). Using the InsideWood web site: potentials and pitfalls. IAWA J. *41*, 412–462.

61. Hijmans, R.J., and van Etten, J. (2012). Raster: geographic analysis and modeling with raster data. R package version *1*, 9–92.

62. Hijmans, R.J., Cameron, S.E., Parra, J.L., Jones, P.G., and Jarvis, A. (2005). Very high resolution interpolated climate surfaces for global land areas. Int. J. Climatol. *25*, 1965–1978.

63. Utescher, T., Bruch, A.A., Erdei, B., François, L., Ivanov, D., Jacques, F.M.B., Kern, A.K., Liu, Y.-S.(C.), Mosbrugger, V., and Spicer, R.A. (2014). The Coexistence Approach—Theoretical background and practical considerations of using plant fossils for climate quantification. Palaeogeogr. Palaeoclimatol. Palaeoecol. *410*, 58–73.

64. Gamisch, A. (2019). Oscillayers: a dataset for the study of climatic oscillations over Plio-Pleistocene time-scales at high spatial-temporal resolution. Glob. Ecol. Biogeogr. *28*, 1552–1560.

65. Fick, S.E., and Hijmans, R.J. (2017). WorldClim 2: new 1km spatial resolution climate surfaces for global land areas. Int. J. Climatol. *37*, 4302–4315.

66. Thuiller, W., Georges, D., Gueguen, M., Engler, R., and Breiner, F. (2021). Biomod2: Ensemble platform for species distribution modeling. R package version 3.5.1. https://cran.r-project.org/package=Biomod2.

67. Hastie, T., Tibshirani, R., and Buja, A. (1994). Flexible discriminant analysis by optimal scoring. J. Am. Stat. Assoc. *89*, 1255–1270.

68. Araújo, M.B., and Guisan, A. (2006). Five (or so) challenges for species distribution modelling. J. Biogeogr. *33*, 1677–1688.

69. Leathwick, J.R., Elith, J., and Hastie, T. (2006). Comparative performance of generalized additive models and multivariate adaptive regression splines for statistical modelling of species distributions. Ecol. Model. *199*, 188–196.

70. Dormann, C.F., Elith, J., Bacher, S., Buchmann, C., Carl, G., Carré, G., Marquéz, J.R.G., Marquéz, G., Lafourcade, B., Leitão, P.J., et al. (2013). Collinearity: A review of methods to deal with it and a simulation study evaluating their performance. Ecography *36*, 27–46.

71. Allouche, O., Tsoar, A., and Kadmon, R. (2006). Assessing the accuracy of species distribution models: prevalence, kappa and the True Skill Statistic (TSS): assessing the accuracy of distribution models. J. Appl. Ecol. *43*, 1223–1232.

72. Breiner, F.T., Nobis, M.P., Bergamini, A., and Guisan, A. (2018). Optimizing Ensembles of Small Models for Predicting the Distribution of Species with Few Occurrences, Edited by Nick Isaac. Methods Ecol. Evol. *9*, 802–808.

STAR★METHODS

KEY RESOURCES TABLE

REAGENT or RESOURCE	SOURCE	IDENTIFIER
Biological samples		
Fossil woods	The Museum of Biology, Sun Yat-sen University, Guangzhou, China	MMHW036; MMHW041; MMHW043
Modern woods	the Wood Collection of Research Institute of Wood Industry, Chinese Academy of Forestry and the Paleoecology Research Group and Center for Gardening and Horticulture, Xishuangbanna Tropical Botanical Garden, Chinese Academy of Sciences	CAFw16669; CAFw12894; CAFw6492; CAFw12151; CAFw12182; CAFw12873; CAFw17698; CAFw6548; XTBG-00,2003,0995; XTBG-00,2009,0262; XTBG-00,2010,0462; XTBG-00,1960,0042; XTBG-00,2002,3291; XTBG-38,1997,0078; XTBG-11,2001,0082
Deposited data		
Species occurrence data	Global Biodiversity Information Facility	https://doi.org/10.15468/dl.2jepdg
Climate data for the late Pleistocene (including 30 ka BP and 20 ka BP)	Oscillayers datasets	https://doi.org/10.5061/dryad.27f8s90
The climate data for modern Maoming Basin	WorldClim version 1.4	http://www.worldclim.org/
Software and algorithms		
Raster package	Hijmans and Etten 2012[1]	http://CRAN.R-project.org/package=raster
Biomod2 R package	Thuiller et al. 2021[2]	https://cran.r-project.org/package=Biomod2

RESOURCE AVAILABILITY

Lead contact

Further questions should be directed to the lead contact, Lu-Liang Huang (571854202@qq.com).

Materials availability

Specimens and permanent microslides of wood sections of fossil woods and extant woods of *Cryptocarya brachythyrsa* (XTBG-00,2003,0995), *C. calcicola* (XTBG-00,2009,0262), *C. depauperata* (XTBG-00,2010,0462), *C. kwangtungensis* (XTBG-00,1960,0042), *C. maculata* (XTBG-00,2002,3291), *C. wrayi* (XTBG-11,2001,0082) and *C. yunnanensis* (XTBG-38,1997,0078) obtained from the Xishuangbanna Tropical Botanical Garden, Yunnan, China (XTBG) are deposited in the Museum of Biology, Sun Yat-sen University, Guangzhou, China. Specimens and wood slices of extant woods of *C. chinensis* (CAFw16669), *C. chingii* (CAFw12894), *C. concinna* (CAFw6492), *C. densiflora* (CAFw12151), *C. griffithii* (CAFw6548), *C. hainanensis* (CAFw12182), *C. impressinervia* (CAFw12873), and *C. metcalfiana* (CAFw17698) are deposited in the Wood Collection of Research Institute of Wood Industry, Chinese Academy of Forestry, Beijing, China (CAFw).

Data and code availability

- All data reported in this paper will be shared by the lead contact upon request.
- No novel code was used in this study.
- Any additional information required to reanalyze the data reported in this paper is available from the lead contact upon request.

EXPERIMENTAL MODEL AND SUBJECT DETAILS

Plants

All specimens used here were obtained as herbarium specimen from the source organizations listed in the key resources table.

METHODS DETAILS

Geological setting

The fossil woods studied here were collected from a stratum of Maoming Basin, located near Zhenjiang Town within Maoming City, Guangdong Province, South China (21.87°N, 110.67°E; Figure 1).

The Maoming Basin, located in southwestern of Maoming, Guangdong Province, hosts one of the largest, mainly Cenozoic, oil shale deposits in China.[53] Previously, plant fossils from Maoming Basin are mainly known from Paleogene deposits,[54,55] with only a few plant fossils reported from Quaternary of Maoming. Recently, a new fossiliferous deposit, lying unconformably on the upper Eocene Huangniuling Formation of Maoming Basin, has been discovered[25] yielding many mummified fossil seeds, fruits, and woods. The deposit is mainly composed of yellow, gray, and black mudstones, grayish yellow and grayish-white fine sandstones, with conglomerate (Figure 1). Accelerator Mass Spectrometry (AMS) ^{14}C dates the plant fossils from this stratum Late Pleistocene (29–27 ka BP, 33–30 ka cal. BP). i.e., MIS (Marine oxygen isotope stage) 3a; work was carried out at the Beta Analytic testing laboratory (Miami, FL, USA).

Taxonomic validation of fossil woods and terminology

The fossil woods in this study were well-preserved by mummification (i.e., minimally altered from their original state),[56] maintaining the cells and tissue systems that were there when the plant was alive; the material is not mineralized and can still be cut as extant wood. These specimens as well as the modern wood samples, were processed and sectioned using the same methods as used for modern wood[57]: They were boiled in water for 12–24 h and soaked in a mixture of ethanol and glycerol for 2 days in order to soften the tissues for sectioning with a microtome (Leica RM2245) at a thickness of 20–30 μm, and then examined with a light microscope (ZEISS AxioScope A1). Wood anatomical measurements and anatomical terminology used for the descriptions in this paper follow the recommendations of the IAWA list of Microscopic Features for Hardwood Identification.[58] The taxonomic position of the fossil woods was determined by comparative work with similar modern and fossil softwood structures. This comparative work was based on modern wood slices and reference materials, particularly the computerized InsideWood database,[23,59] in which we can search for similar modern softwoods by entering an IAWA feature number followed by the coding letters such as p (present), a (absent), r (present required), and e (absent required). To avoid the limitations of the InsideWood webresource,[60] we also consulted other reference materials (such as literature descriptions and wood slices), as well as examined the anatomical structures of related extant wood of *Cryptocarya* to verify the identification.

Wood anatomical study of extant *cryptocarya* species from China and Malaysia

As the information on wood anatomy of most species of *Cryptocarya* from eastern Asia is not availabe to date, we examined the wood structure of 15 species of this genus from China and Malaysia (see Table S1). Among them, 11 species have never been studied by wood anatomists. We described the wood structure on the microslides of *C. chinensis*, *C. chingii*, *C. concinna*, *C. densiflora*, *C. hainanensis*, *C. impressinervia*, *C. metcalfiana*, and *C. griffithii* (8 species) from the Wood Collection of Research Institute of Wood Industry, Chinese Academy of Forestry (CAFw). 7 wood samples of *C. brachythyrsa*, *C. calcicola*, *C. depauperata*, *C. kwangtungensis*, *C. maculata*, *C. yunnanensis* and *C. wrayi* has been obtained from the Paleoecology Research Group and Center for Gardening and Horticulture, Xishuangbanna Tropical Botanical Garden, Chinese Academy of Sciences (XTBG), and permanent microslides have been made using standard methods (see "taxonomic validation of fossil woods and terminology"). As the wood samples were not available for most *Cryptocarya* species, we did not measure the length of vessel elements and libriform fibers on the macerated wood.

QUANTIFICATION AND STATISTICAL ANALYSIS

Climatic data collection

We assessed the average, minimum and maximum values of 19 bioclimatic parameters for the modern distribution ranges of *Cryptocarya chinensis* (Hance) Hemsl (see Table S2). The values for the bioclimatic variables were based on the coordinates of 249 species occurrences retrieved from the Global Biodiversity Information Facility (GBIF) web portal (http://www.gbif.org/, GBIF.org (2 November 2022) GBIF Occurrence Download https://doi.org/10.15468/dl.2jepdg) (see Figure S4). The Raster package[61] in R was used to extract from this dataset 19 bioclimatic variables representing ranges of temperature and precipitation for each occurrence as recorded in the WorldClim climate layers at a resolution of 2.5 arc-min.[62]

The climate data for the Late Pleistocene (including 30 ka and 20 ka) and the modern Maoming Basin were reconstructed using the Coexistence Approach (CA,[63]) based on Maoming fossil data (30 ka), extracted from the Oscillayers datasets[64] (30 ka and 20 ka) and WorldClim version 1.4[62] at a resolution of 2.5 arc-min (modern).

Biomod2 ensemble species distribution modeling

The nineteen bioclimatic variables for both modern and paleo-climate obtained from WorldClim[65] (modern) and Oscillayers[64] (30 ka, 20 ka) were used to model the potential ancient species distribution of *Cryptocarya chinensis* in eastern Asia (longitude: 100°E–125°E, latitude: 10°N–35°N) by means of the Biomod2 R package.[66] Biomod2 combines various statistics-based and machine learning-based species distribution modeling algorithms to predict optimized the habitat suitability estimation.[67–69] Species occurrence data were collected from the Global Biodiversity Information Facility (GBIF: http://www.gbif.org/) and Flora Reipublicae Popularis Sinicae (FRPS: https://www.iplant.cn/frps).

Climatic variable processing

Bioclimatic variables with significant mutual correlation (high multicollinearity) could affect the performance of the model.[70] Thus, we excluded variables with Pearson correlation value greater than 0.96, and took into consideration empirical knowledge about the importance of different climate variables. After this filtering procedure, 9 variables were retained for modeling the distribution of *Cryptocarya chinensis*: mean diurnal range (BIO2, °C), isothermality (BIO3), temperature seasonality (BIO4), mean temperature of wettest quarter (BIO8, °C), annual precipitation (BIO12, mm), precipitation of wettest month (BIO13, mm), precipitation seasonality (BIO15), precipitation of warmest quarter (BIO18, mm), and precipitation of coldest quarter (BIO19, mm).

Model establishment

The ensemble model was run initially with ten algorithms, including artificial neural networks (ANN), surface range envelope (SRE), flexible discriminant analysis (FDA), general linear models (GLM), general additive models (GAM), general boosted models (GBM), classification tree analysis (CTA), multiple adaptive regression splines (MARS), random forests (RF), and maximum entropy (MaxEnt. Phillips.2) model. Five models were finally selected for the run according to ROC (receiver operating characteristics) (>0.85) and TSS (true skill statistics) thresholds (>0.95), i.e., "MaxEnt. Phillips.2", "FDA", "RF", "MARS", "GBM".

A random selection of 80% of the modern presence-pseudoabsence data of *Cryptocarya chinensis* (retrieved from GBIF as described above) was used to train each SDM 10 times (for a total of 100 runs for the 10 algorithms), and the remaining 20% was used for cross-validation, with ROC, and TSS measured for evaluation.[71,72]

The ensemble SDM was used for projecting the modern and past suitable habitat ranges of *Cryptocarya chinensis*, including at 30 ka (the present fossil record), 20 ka (Last Glacial Maximum, LGM), and 0 ka (modern).